Optical imaging of visually evoked responses in prosimian primates reveals conserved features of the middle temporal visual area

Xiangmin Xu*, Christine E. Collins*, Peter M. Kaskan*, Ilya Khaytin†, Jon H. Kaas*‡, and Vivien A. Casagrande*†‡§¶

Departments of *Psychology, ‡Cell and Developmental Biology, and §Ophthalmology and Visual Sciences and †Medical Sciences Training Program, Vanderbilt University, Nashville, TN 37232

Contributed by Jon H. Kaas, December 31, 2003

Optical imaging of intrinsic cortical responses to visual stimuli was used to characterize the organization of the middle temporal visual area (MT) of a prosimian primate, the bush baby (*Otolemur garnetti*). Stimulation with moving gratings revealed a patchwork of oval-like domains in MT. These orientation domains could, in turn, be subdivided into zones selective to directional movements that were mainly orthogonal to the preferred orientation. Similar, but not identical, zones were activated by movements of random dots in the preferred direction. Orientation domains shifted in preference systematically either around a center to form pinwheels or as gradual linear shifts. Stimuli presented in different portions of the visual field demonstrated a global representation of visual space in MT. As optical imaging has revealed similar features in MT of New World monkeys, MT appears to have retained these basic features of organization for at least the 60 million years since the divergence of prosimian and simian primates.

The cerebral cortex of all studied primates contains a number of functionally distinct visual areas, but only a few of these areas are so well defined that they are widely recognized as present in all primates. These areas include primary and secondary visual areas (V1 and V2, respectively), which appear to be characteristic of nearly all mammals, and the middle temporal visual area (MT, also termed V5), which has been identified only in primates (1). The restricted distribution suggests that MT appeared as a distinct visual area with, or just before, the emergence of the first primates. Comparative studies have identified a number of features of MT that are present in all studied primates and thus are likely to have been conserved since the last common ancestor. MT receives direct inputs from V1, contains a crude but characteristic representation of the contralateral visual hemifield, has dense myelination, and contains a preponderance of neurons selective for direction of stimulus movement (1). Here, we address the question of what additional features are likely to be conserved from early primate ancestors. To do so, we use the method of optical imaging of intrinsic signals in MT of prosimian bush babies (*Otolemur garnetti*, also termed *Galago garnetti*) that are evoked by different stimulus conditions. Prosimian primates represent a major branch of primate evolution that diverged from the anthropoid branch (monkeys, apes, and humans) >60 million years ago (2). As optical imaging has been used to extensively characterize the functional organization of MT in a New World monkey, the owl monkey (3), it is possible to compare MT in this simian and prosimian bush babies in detail and identify ancient, ancestral features that are common to both lines of evolution.

Materials and Methods

General Preparation. The three bush babies (greater galagos, now referred to as *O. garnetti*) used in this study were handled according to an approved protocol from the Vanderbilt University Animal Care and Use Committee. Basic procedures have been described (4). Briefly, bush babies were initially anesthetized with isoflurane (2–4% in O_2), and paralysis was induced by i.v. injection of 1–1.5 mg/kg vecuronium bromide. Bush babies were artificially ventilated with a mixture of 75% N_2O and 25% O_2 delivered at a rate sufficient to maintain the peak end tidal CO_2 level at ≈4%. Paralysis and anesthesia were maintained by i.v. infusion of vecuronium bromide (0.2–0.4 mg/kg per h) mixed in 5% dextrose lactated Ringer's solution and propofol (10–20 mg/kg per h) through separate lines. Pupils were dilated with atropine, and gas-permeable contact lenses rendered the retina conjugate with the 28.5-cm-distant stimulus monitor. During experiments the optic disks and *areae centralii* (ACs) were plotted on the screen, and 3-mm artificial pupils were placed in front of the eyes. A craniotomy exposed MT and surrounding visual areas, and openings were sealed with 1% agarose under a glass coverslip.

Visual Stimuli and Optical Imaging. The functional organization of MT was imaged in five hemispheres in three bush babies. Each experimental session lasted from 36 to 60 h. Intrinsic optical imaging signals were acquired with the IMAGER 2001 differential video-enhancement imaging system and VDAQ/NT data acquisition software (Optical Imaging, Mountainside, NJ). Surface reference images of cortical vasculature were acquired with a 540-nm green light. The cortex was illuminated with either 611 or 689 nm of light during data acquisition and was visualized with a tandem lens macroscope attached to a low-noise video camera. Visual stimuli were generated by using a VSG system (Cambridge Research Systems, Rochester, U.K.) and were presented on a 21-inch (1 inch = 2.54 cm) video screen (Sony FD Trinitron, model GDM-F400) in 120-Hz noninterlaced mode with a mean luminance of 30 cd/m^2.

For visuotopic mapping, different and restricted sizes of stimuli, unless otherwise specified, were presented monocularly at different visual field locations at eccentricities ranging from 0° to 40°. Stimuli consisted of drifting gratings (fundamental spatial frequency, 0.2 cycles per degree; drift velocity, 2 Hz; duty cycle, 20%) presented at two orientations of 0° and 90°, inside the spatially restricted stimuli such as circles, rings, wedges, and rectangles. The stimuli were positioned relative to the projection of the AC of the retina into the contralateral visual field.

To study responses to stimuli of different orientations, high-contrast rectangular gratings (fundamental spatial frequency 0.2–0.4 cycles per degree; drift velocity, 2 Hz; duty cycle, 20%) of four orientations at intervals of 45° were displayed on the full screen and presented binocularly. Each grating was moved back and forth along an axis that was orthogonal to the orientation of the grating. A single trial consisted of data acquisition during continued presentation of the drifting grating stimulus for 8 s and an interstimulus interval of 12 s using a blank screen of mean

Abbreviations: V1, primary visual area; V2, secondary visual area; MT, middle temporal visual area; AC, *area centralis*.

¶To whom correspondence should be addressed. E-mail: vivien.casagrande@vanderbilt.edu.

www.pnas.org/cgi/doi/10.1073/pnas.0308745101

luminance. Stimulus sets were made up of 10–30 trials. To study responses to different directions of motion, high-contrast rectangular gratings were moved in eight directions at intervals of 45° on the full screen, presented binocularly. In addition, high-contrast randomly positioned dots were drifted in eight different directions (dot size, 0.07° × 0.07°; dot density, 3–6% surface area; dot speed, 10° per s) within a circular window of 20°–30° centered on the AC representation and viewed binocularly.

Video images were acquired at a rate of 30 frames per s, but all frames acquired for each condition during the 8-s period were summed together for eight data frames before further analysis. Individual data frames included 744 × 480 pixels, with a resolution of 87 pixels per mm.

Image Analysis. Two approaches were used to create visuotopic activation maps. At each mapping location, one set of stimulus conditions consisted of two different orientations for the same position and one control blank (mean luminance gray screen). By using WINMIX software (Optical Imaging), all activity images associated with stimuli of the same orientation were summed and divided by the "pure blank" obtained by summing the images of the blank control to create single-condition maps. In addition, the summed activity images acquired during the presentation of one orientation were divided by the summed activity images acquired during presentation of the orthogonal orientation to create differential maps (5). Custom programs written in MATLAB were used to further process the data. The resulting maps were routinely "clipped" (1.5–2 SDs around the mean), smoothed by using a Gaussian kernel of two to three pixels, and scaled in the range of 0–255 gray levels for appropriate display. No further processing was done unless specified.

To construct maps of direction preference, all images associated with the same stimulus direction (drifting gratings or random dots) were summed. The summed images acquired during the presentation of one direction were divided by a "mixture" blank (the average summed images of all of the stimulus directions) to create single-direction maps (3). We also created differential-direction maps by dividing the images associated with one direction by those associated with the opposite direction. Similarly, orientation differential maps were created by dividing the images associated with one orientation by those associated with the orthogonal orientation.

Orientation and direction preference maps were smoothed by using a 7 × 7-pixel mean filter kernel. Low-frequency noise was reduced by convolving the image with an 80 × 80-pixel mean filter kernel and subtracting the result from the original image. Filtering was done in the floating point range before the maps were clipped and scaled in the range of 0–255 gray levels. Vector summation of the orientation or direction maps on a pixel-by-pixel basis was used to create a color-coded orientation or direction preference (angle) map. A magnitude map of the degree of orientation or direction selectivity was coded by brightness, with strong orientation or direction selectivity being the brightest (see ref. 6 for details). The two maps were combined to create a polar map, which contains information about both orientation or direction preference (color) and magnitude of selectivity (brightness).

To reduce vascular artifacts, we used a stack of optical images to create a mask indicating the location of the major blood vessels. The grayscale value for each pixel within the mask was replaced by the mean of the grayscale values of the appropriate surrounding pixels outside the mask (7, 8).

Histology and Alignment. At the termination of each experiment, the bush baby was deeply anesthetized with an overdose of sodium pentobarbital and perfused transcardially with 0.9% saline in 0.1 M phosphate buffer (PB) followed by 2% paraformaldehyde in 0.1 M PB. The brain was removed, and the cortex was separated and flattened. The cortex was frozen and cut with the surface vascular pattern preserved in the first 100-μm section. Subsequent sections were cut at 40 μm. Sections were processed for cytochrome oxidase (9) and myelin (10).

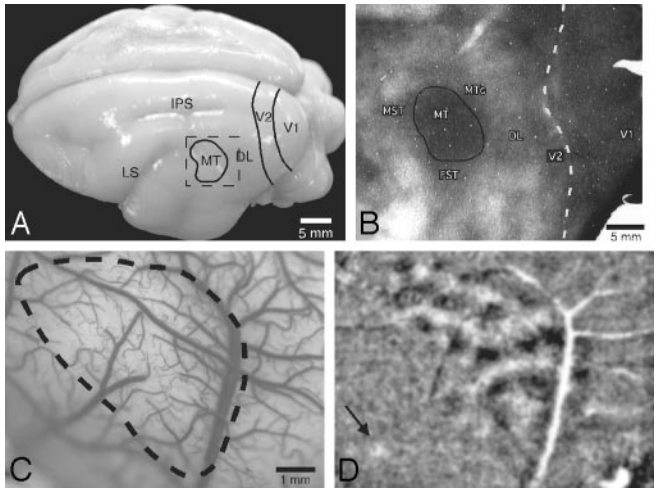

Fig. 1. Visualization of MT *in vivo* by optical imaging of intrinsic signals. (*A*) A dorsolateral view of the bush baby brain showing approximate locations of V1, V2, the dorsolateral area (DL), and MT is shown. The dashed box indicates the estimated camera view for the optical images acquired in case 03-01. The intraparietal sulcus (IPS) and lateral sulcus (LS) are also indicated. (*B*) A section of flattened cortex stained for myelinated fibers is shown with architectonically defined boundaries of MT and surrounding areas. MST, medial superior temporal area; FST, fundal superior temporal area; MTc, MT crescent. (*C*) The cortical surface of the imaged area, showing the blood vessel pattern and the approximate boundary of the MT (dashed line), which was revealed by activation patterns resulting from binocular stimulation of full-screen drifting gratings at four different orientations (0°, 45°, 90°, and 135°). (*D*) Shown is one of the orientation differential maps (90°/0°) (case 03-01). Dark patches are areas with selective responses to orientation 90°; white patches are areas with selective responses to orientation 0°. The region highly responsive to oriented, drifting gratings closely approximates MT as identified architectonically in the same case. Less pronounced activity occurs in surrounding cortex. The arrow marks a small focus of activity rostrolateral to MT. (Scale bar for *C* and *D* is shown in *C*.)

Surface and radial blood vessels were the primary landmarks used to align histological sections with the optical reference images of the imaged area. Differences between images and sections caused by distortion or tissue shrinkage (≈10–15%) were handled by global scaling and rotation. After the optical images were aligned with the histological data, we examined the corresponding locations or patterns of the imaged brain areas to see whether anatomical delineation of MT matched with optical imaging results. In each case, the cytochrome oxidase and myelin patterns identified boundaries of MT that were consistent with those estimated from imaging results.

Results

The optical imaging procedures allowed us to extensively characterize MT in bush babies and produce several major findings. The first major finding was that MT was activated by drifting gratings of different orientations in ways that clearly distinguished MT from surrounding areas. MT is located in the middle of the upper temporal lobe of bush babies (Fig. 1*A*), where it can be delimited as a myelin-dense area (Fig. 1*B*). The densely myelinated region of cortex was strongly activated when full-screen (40°) drifting gratings were viewed. The activation pattern was patchy or modular across the surface of MT (Fig. 1*D*), and the locations of activated patches varied with the orientations of the drifting gratings (see below). The full-screen grating most strongly activated the dorsocaudal two-thirds of MT, represent-

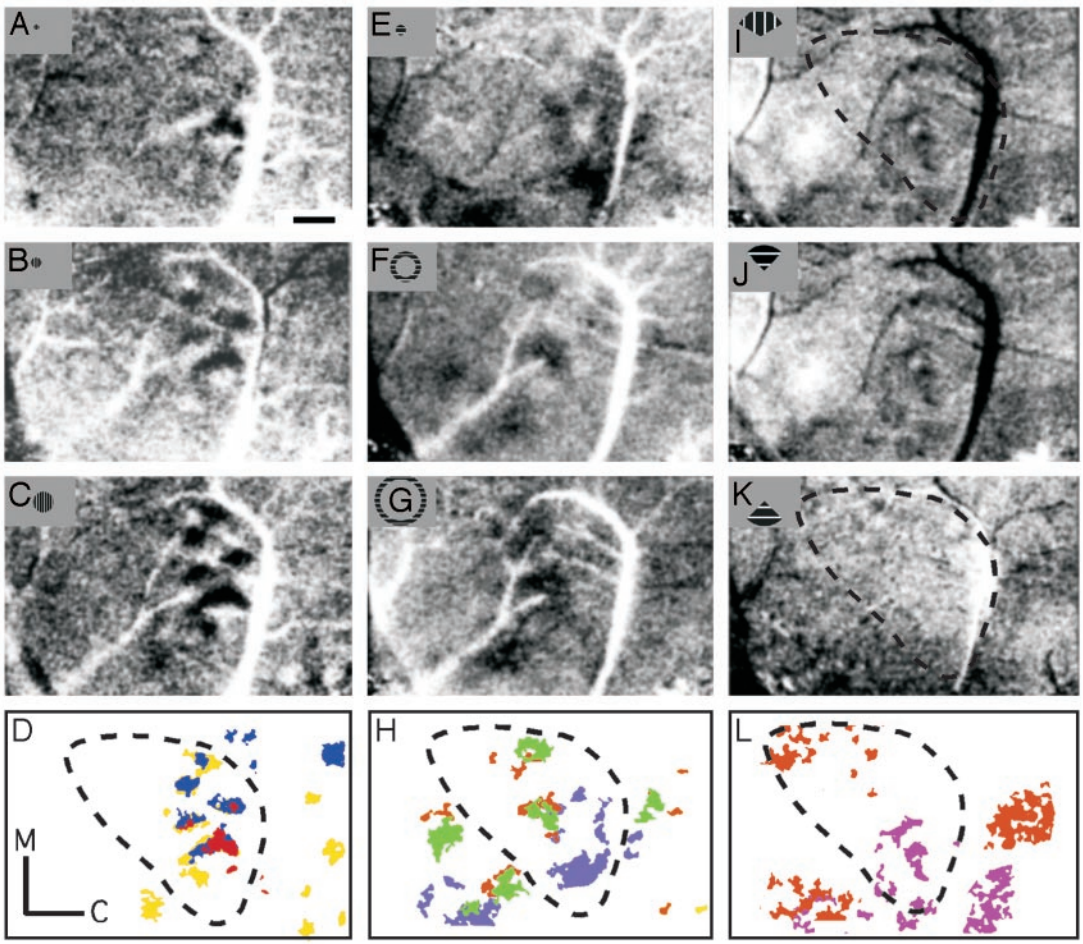

Fig. 2. The retinotopic organization of MT and surrounding cortex revealed by stimuli restricted to part of the visual field is shown. (*A–D*) Differential activation maps (0°/90°) resulting from binocular stimulation of drifting gratings in a disk centered on the representation of AC: 2.5° (radius) disk (*A*), 5° disk (*B*), and 10° disk (*C*). Note that differential maps tend to show the most robust activation patterns. (*D*) Summary of high-activity patterns (red, 2.5°; blue, 5°; yellow, 10°) is shown. M, medial; C, caudal. (*E–G*) Single-condition maps resulting from monocular stimulation of drifting vertical gratings in a 5° radius disk (*E*), a 10–15° annulus (*F*), and a 20–25° annulus (*G*) are shown. All are centered on the representation of the AC. (*H*) High-activity patterns are summarized (5°, blue; 10–15°, green; 20–25°, orange). (*I–L*) Shown are activation patterns resulting from stimulation by a wedge in the upper visual field [120° wedge (*I*) and 90° wedge (*J*), radius = 25°] and a wedge in the lower visual field [90° wedge (*K*), radius = 25°] with the apex centered on the AC. (*L*) Summary of high-activity patterns from *I–J* (upper field in violet, lower field in orange) is shown. All of the optical images here are from the same case as in Fig. 1 (case 03-01). The dashed contours in *D*, *H*, and *L* indicate the approximate MT extent. (Scale bar in *A* is 1 mm.)

ing central and paracentral vision, with little or no activation in the ventrorostral third of MT, representing peripheral vision beyond the 40° of the stimulus screen. Although some areas beyond MT showed activation (Fig. 2), none of the areas of cortex surrounding MT were as highly activated by the gratings, indicating that such stimuli effectively distinguish MT and identify most of its extent (Fig. 1*D*). Defined by imaging, the size of MT (18 mm^2 with a rostrocaudal length of 4.1 mm and a dorsoventral height of 6.3 mm) corresponds with previous portrayals of MT in bush babies (11, 12) and with the size of MT judged from histological boundaries in the present cases (Fig. 1*D*).

The second major finding was that stimuli restricted to parts of the visual field effectively revealed features of the retinotopic organization of MT. The overall retinotopic organization of MT in bush babies (13) and other primates (13, 14) is known from relating receptive field locations of neurons to recording sites in MT, but optical imaging provides a richer understanding of the ways that stimuli in different parts of the visual field activate MT. Oriented drifting gratings of only a few degrees of visual angle continued to strongly activate small patches in MT. As few as one to three patches were well activated, with the location of the patches dependent on where in the visual field the stimulus was presented (Fig. 2*A*). Successively larger stimuli activated successively larger arrays of patches (compare Fig. 2 *A–C*), and similarly located stimuli of different orientations activated different patches in the same cortical region (compare Fig. 2 *B* and *E*). Gratings that changed from a small disk in central vision to larger and larger rings activated patches that progressed rostrally in MT (Fig. 2 *E–H*), whereas gratings in the lower visual field activated patches in MT dorsal to those activated by upper field gratings (Fig. 2 *I–L*). These results demonstrate the effects of varying stimulus location and orientation when stimulating MT and indicate that at least several patches of neurons are highly activated by small, restricted stimuli. An additional result is that spatially restricted stimuli activate patches of cortex outside of MT, although less strongly, and that these patches appear to be parts of additional retinotopic areas (Fig. 2 *D*, *H*, and *L*). These patches likely reflect activity in the proposed visual areas medial superior temporal area, fundal superior temporal area, MT crescent, and the dorsolateral area (Fig. 1*B*).

Consistent with the greater magnification of central vision in MT (11), restricted stimuli of the same size activated more

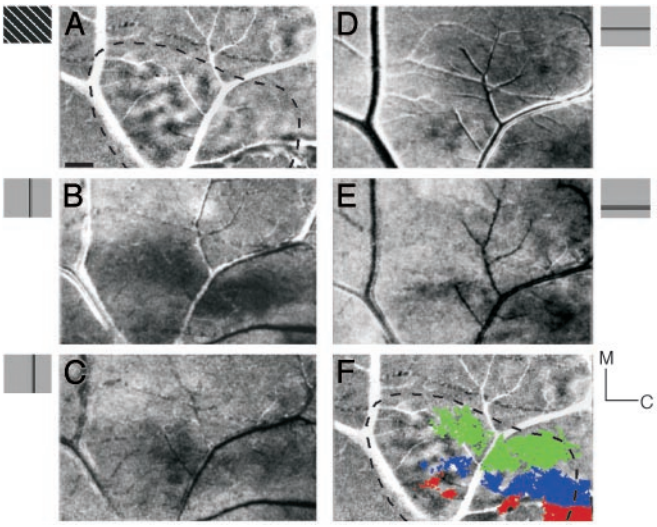

Fig. 3. The retinotopic organization of MT revealed by drifting gratings in horizontal or vertical windows in different locations is shown. (*A*) The extent of MT (dashed line, case 03-02) was revealed by full-screen stimulation with a drifting grating (135°/45° differential map). (*B* and *C*) Activity patterns as the 4° vertical window is shifted from centered on the vertical meridian (*B*) to 4° to the right (*C*). (*D–F*) Activity patterns as the horizontal window is shifted from 0° horizontal (*D*) to −8° (*E*). (*F*) Colorized, thresholded images of activation resulting from 0° vertical meridian stimulation (green), 0° horizontal meridian (HM) stimulation (red), and 8° below HM stimulation (blue) M, medial; C, caudal. (Scale bar is 1 mm.)

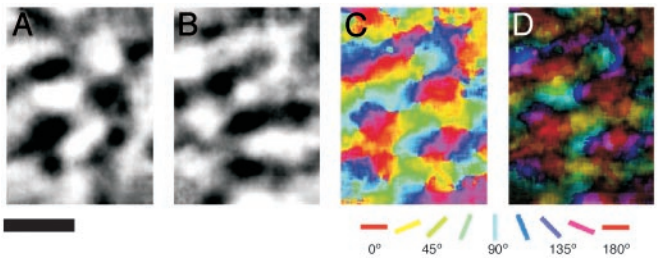

Fig. 4. Functional maps of orientation preference in MT from case 03-02 are shown. Orientation differential maps were obtained from full-field, drifting gratings at four orientations with 0°/90° (*A*) and 45°/135° (*B*) (90°/0° and 135°/45° are not shown). Dark areas responded strongly to the first orientation, whereas light areas responded strongly to the second, orthogonal grating orientation. (*C*) A color-coded orientation preference map was produced from vector summation on a pixel-by-pixel basis from the four differential maps noted above. The key shown below the map indicates orientation preference. (*D*) The polar map of orientation preference contains information about both orientation preference (color) and magnitude of orientation selectivity (brightness, dark to light = weak to strong). (Scale bar is 1 mm.)

cortical tissue in MT when presented in the central, compared with the peripheral, visual field, and activations produced by adjacent stimuli overlapped more in the representation of paracentral and peripheral vision.

Other aspects of the visuotopic organization relative to orientation domains in MT were revealed by comparing activation patterns produced by full-screen stimulation with those by vertical or horizontal slit-like windows of stimulation. Again, the full-screen (40°) grating activated patches over most of MT (Fig. 3*A*), whereas a narrow (4°) vertical window centered on the vertical meridian through the center of the gaze activated a broad strip of MT along its outer border (Fig. 3*B*), where the vertical meridian is represented (11, 13). The vertical meridian stimulus also activated regions well into MT, indicating that the responsive neurons are not tightly confined to the MT border. Moving the vertical window 4° into the contralateral visual hemifield produced only a modest shift in activation away from the upper border of MT (Fig. 3*C*). Narrow horizontal windows of stimulation also activated patchy bands of tissue in MT, with the band activated by a window on the zero horizontal meridian (Fig. 3*D*) located more ventral than the band activated by the horizontal window displaced 8° into the lower visual quadrant (Fig. 3*E*). The color-coded summary in Fig. 3*F* illustrates that the band activated by the zero vertical window (green) was most dorsal in MT along the dorsal border devoted to the lower visual quadrant (the ventral border of MT would also be expected to be activated by this stimulus, but it was out of the view of the camera). In contrast, the red band corresponds to the zero horizontal activation zone, effectively dividing MT into dorsal and ventral halves. The −8° horizontal window shifted the band of activation (blue) into the dorsal half of MT, as predicted by microelectrode studies of retinotopy (11). However, the retinotopy revealed by optical imaging was crude, with restricted stimuli activating large portions of MT and spatially adjacent stimuli activating largely overlapping regions.

Although all of the stimulus presentations with oriented gratings demonstrated a patchy distribution of highly activated tissue, the relationship of sets of patches activated by different orientations to each other was most effectively illustrated by orientation maps. These maps were produced by dividing activity patterns from orthogonal orientations (Fig. 4 *A* and *B*) and combining results based on different orientations in a single color-coded summary. The summary shows how systematic rotations of stimulus orientations produce systematic shifts in activation patterns, with clusters of activation for orientation arrays corresponding in number to the activation patches for any orientation (Fig. 4*C*). The isoorientation domains formed elongated ovals (see Figs. 1*D* and 4 *A* and *B*). The average size of the isoorientation domains of the four orientations was 0.2 ± 0.015 mm^2 (mean ± SD). The isoorientation domains shifted from one to the next in orientation pinwheels, where orientation preference changes in a radial fashion around a single point, and linear zones, where orientation preference changes slowly along a straight line (Fig. 4*C*). When activation strengths for all orientations were considered, the surface-view map was divided into an additional patchwork of highly activated and poorly activated territories. This finding suggests that MT of bush babies has a second type of modular organization consisting of a patchwork of regions of poor orientation tuning where neurons are not highly sensitive to moving, oriented gratings. Single-neuron recordings and 2-deoxyglucose labeling patterns in owl monkey suggest that MT contains segregated modular groups of neurons more effectively activated by either global or local motion (15, 16). The gratings and arrays of moving dots in the present experiments may have best activated the MT modules sensitive to global motion.

The orientation maps of MT reflect the movement of oriented stimuli back and forth in two opposite directions. A further finding of the present study was that the movement of an oriented stimulus in one direction did not activate the same territories as movement in the opposite direction (Fig. 5 *A* and *B*). Instead, patches of MT best activated by a particular orientation were divided into parts preferring motion in one direction or the other (Fig. 5*C1*). In general, isoorientation domains had a more band-like appearance and were typically larger in size and more uniform in their distribution than isodirection domains. In a way similar to the color-coded orientation preference map (Fig. 5*C2*), the color-coded direction preference map (Fig. 5*C3*) consisted of numerous regions within which direction preference changes in a slow, continuous fashion. There were also some

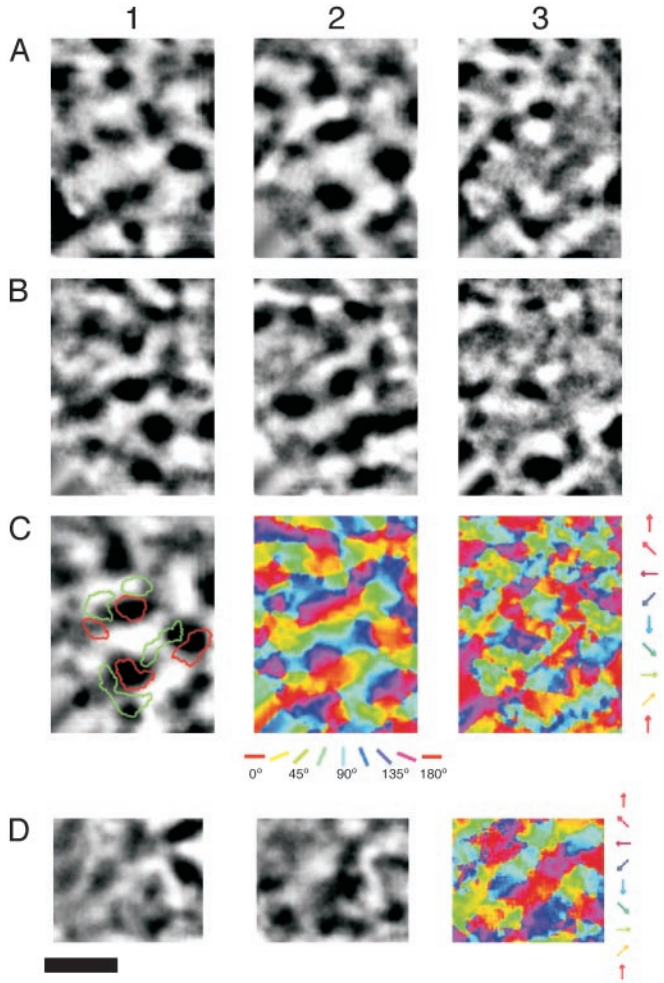

Fig. 5. The relation of orientation preference maps to direction-of-movement maps in MT (case 03-02) is shown. The regions illustrated in *A–C* are identical. *D* is from a different region of MT. (*A*) Single-condition direction of movement maps for upward, 0° (*1*) and downward, 180° (*2*) grating movement, and the differential direction-of-movement map (upward/downward) (*3*). (*B*) Single-condition direction-of-movement maps for upward oblique (*1*) and downward oblique (*2*) gratings of the same orientation and the differential direction-of-movement map (*3*) (upward oblique, 135°/downward oblique, 315°). In *A3* and *B3*, the dark regions correspond to particular isodirection domains, and the white regions correspond to the opposite isodirection domains. (*C1*) Orientation differential map (0°/90°) with selected contours of isodirection domains from *A3* (90° isodirection domains, green; 270° isodirection domains, red). (*C2*) An orientation preference map, created from vector summation of four orientation differential maps. (*C3*) A direction preference map, created from vector summation of eight differential direction-of-movement maps (e.g., 90°/270° and 135°/315°shown in *A3* and *B3*). (*D1* and *D2*) Single-condition maps of direction of movement from moving random dot stimuli in the directions of 0° and 180°. (*D3*) A color-coded direction preference map from vector summation of eight single-condition maps of direction resulting from random dot stimuli moving in eight different directions. (Scale bar is 1 mm.)

regions separated by winding boundaries across which direction preference shifted abruptly, often by 180°. The vertical and horizontal direction preference domains appeared to account for a large portion of the cortical map (Fig. 5*C3*).

MT also demonstrated direction selective domains when stimulated by moving random dot patterns (Fig. 5*D 1* and *2*), although random dots induced weaker responses than directional grating stimuli. Nevertheless, the direction preference map produced with dots shared similar, but not identical, features to that produced from the gratings (Fig. 5*D3*).

Discussion

The present results indicate that MT of prosimian bush babies is functionally organized in a manner very similar to MT of simian primates. In the present optical imaging experiments, moving gratings selectively activated arrays of orientation preference domains across MT. Sequences of orientation preference domains systematically rotated around pinwheel centers or changed along a straight line, with each orientation domain divided into territories for opposite directions of movement preference. Moving arrays of random dots activated similar direction of movement territories. Nearly full-hemifield (40°) stimuli strongly activated most of MT, whereas stimuli restricted to smaller portions of the contralateral hemifield activated restricted areas of MT in a global retinotopic pattern. Overall, these results are remarkably similar to optical imaging results reported for MT of owl monkeys, a New World monkey (3), results that are highly consistent with data from microelectrode recording experiments in New World cebus monkeys (17) and Old World macaque monkeys (18–24). As prosimian and anthropoid (monkeys, apes, and humans) lines of primate evolution diverged >60 million years ago, and New World and Old World monkeys separated some 40 million years ago (2), the basic features of MT organization appear to have emerged at least 60 million years ago, and these features have been conserved in three major lines of primate evolution. Thus, specialized cortical circuits in MT for processing direction of stimulus motion emerged early and were conserved in primate evolution. These circuits remain embedded in a global retinotopic framework that presumably allows a spread of activation in MT so that any direction of stimulus motion in any location in the visual field can effectively engage some circuits. Below, we consider these key results in relation to findings previously reported.

Visuotopy in MT. Our optical imaging results in bush baby MT demonstrate the existence of an orderly retinotopic map, confirming results of earlier microelectrode mapping studies in this prosimian primate (11), New World owl monkeys, cebus monkeys, and marmosets (11, 13, 25, 26), and Old World macaque monkeys (14, 27). The existence of such an orderly map is also supported by anatomical studies tracing connections from V1 in a number of prosimian and simian primates including bush babies (28), squirrel monkeys (29), owl monkeys (30), marmosets (31), and macaque monkeys (32). In bush babies, the mapped region of MT (0–40°) always corresponded to the area judged to be MT based on dense myelin and cytochrome oxidase staining. In Old World simians such as macaque monkeys and in humans reports have been conflicting concerning whether visuotopy is smooth and orderly and whether all of MT corresponds in macaque monkeys to the area of densest myelin or cytochrome oxidase staining. Functional MRI has been used to provide evidence of visuotopy in MT of humans, although such a map is not always apparent because of resolution issues (33). Thus it seems reasonable to conclude that there is an orderly visuotopic map of the contralateral visual hemifield in MT of all primates.

Modular Organization of Orientation and Direction. Orientation domains in MT of bush babies are organized very much like those of V1 in monkeys, being represented continuously as a series of pinwheels and linear zones. However, the orientation domains in MT (≈0.2 mm^2) are much larger than those in V1 (≈0.09 mm^2). A very similar organization for orientation domains was reported for MT in owl monkeys by using optical imaging procedures (3). This arrangement of orientation contrasts with that described in V2 and V3 of simians where domains of high orientation selectivity are separated by distinct bands of low orientation selectivity (unpublished data). Although orientation domains have been examined only in bush babies and owl

monkeys, microelectrode recordings from both New World and Old World monkeys have previously demonstrated that a majority of neurons in MT are well tuned for orientation (19–20, 22), although this is not widely recognized. Our data in bush babies also demonstrate that regions surrounding MT, including both the MT crescent and medial superior temporal area, contain cells selective for orientation as reported by others in owl monkeys and macaque monkeys (4, 34, 35).

Our results demonstrate a systematic representation of direction of stimulus movement in MT of bush babies that is similar to that demonstrated by using optical imaging in New World owl monkeys (3) and by electrophysiological recording in New World cebus monkeys (17). In Old World macaque monkeys, directionally selective cells also are clearly organized into columns in MT (22, 36). In cebus monkeys, owl monkeys, and bush babies, stimulus direction appears to be represented by continuous changes in directional preference, as well as by breaks and points where there are rapid changes in direction (pinwheel-like). This arrangement of directional domains is similar to that identified for directional domains in cat area 18 (37, 38) and ferret area 17 (39). This representation of direction is somewhat different from the rectilinear model proposed for the organization of direction in macaque monkey MT by Albright *et al.* (36), a difference that likely reflects the difficulties inherent in reconstructing surface-view maps from single-unit recordings within a structure buried in a sulcus. Thus, in a fashion analogous to V1 (40), optical imaging has revised our view of the geometry of feature representations in MT. In addition, optical imaging studies in owl monkeys (3) and bush babies (present study) provide clear evidence that the basic organization of MT emerged with or before early primates and has been retained in both prosimian and anthropoid lines of descent.

We thank Anna Roe for helpful comments on the manuscript and Daniel Shima and Mary Feurtado for excellent technical assistance. This work was supported by National Eye Institute Grants EY01778 (to V.A.C.), and EY02685 (to J.H.K.), Core Grants from the National Eye Institute (EY08126) and the National Institute of Child Health and Human Development (HD 15052), and National Center of Research Resources Shared Instrumentation Grant 1S10RR13947 (to V.A.C.).

1. Kaas, J. H. (2004) in *The Primate Visual System*, eds. Kaas, J. H. & Collins, C. E. (CRC, Boca Raton, FL), pp. 139–159.
2. Purvis, A. (1995) *Philos. Trans. R. Soc. London B* **348,** 405–421.
3. Malonek, D., Tootell, R. B. H. & Grinvald, A. (1994) *Proc. R. Soc. London Ser. B* **258,** 109–119.
4. Lyon, D. C., Xu, X. M., Casagrande, V. A., Stefansic, J. D., Shima, D. & Kaas, J. H. (2002) *Proc. Natl. Acad. Sci. USA* **99,** 15735–15742.
5. Blasdel, G. G. (1992) *J. Neurosci.* **12,** 3115–3138.
6. Bosking, W. H., Zhang, Y., Schofield, B. & Fitzpatrick, D. (1997) *J. Neurosci.* **17,** 2112–2127.
7. Bosking, W. H., Kretz, R., Pucak, M. L. & Fitzpatrick, D. (2000) *J. Neurosci.* **20,** 2346–2359.
8. Blasdel, G. & Campbell, D. (2001) *J. Neurosci.* **21,** 8286–8301.
9. Wong-Riley, M. (1979) *Brain Res.* **171,** 11–28.
10. Gallyas, F. (1970) *Acta Neuropathol.* **16,** 35–38.
11. Allman, J. M., Kaas, J. H. & Lane, R. H. (1973) *Brain Res.* **57,** 197–202.
12. Beck, P. D. & Kaas, J. H. (1998) *J. Comp. Neurol.* **398,** 162–178.
13. Allman, J. M. & Kaas, J. H. (1971) *Brain Res.* **31,** 85–105.
14. Van Essen, D. C., Maunsell, J. H. & Bixby, J. L. (1981) *J. Comp. Neurol.* **199,** 293–326.
15. Born, R. T. & Tootell, R. B. (1992) *Nature* **357,** 497–499.
16. Born, R. T. (2000) *J. Neurophysiol.* **84,** 2658–2669.
17. Diogo, A. C., Soares, J. G., Koulakov, A., Albright, T. D. & Gattass, R. (2003) *J. Neurosci.* **23,** 3881–3898.
18. Felleman, D. J. & Kaas, J. H. (1984) *J. Neurophysiol.* **52,** 488–513.
19. Zeki, S. (1980) *Proc. R. Soc. London Ser. B* **207,** 239–248.
20. Baker, J. F., Petersen, S. E., Newsome, W. T. & Allman, J. M. (1981) *J. Neurophysiol.* **45,** 397–416.
21. Allman, J., Miezin, F. & McGuinness, E. (1985) *Perception* **14,** 105–126.
22. Albright, T. D. (1984) *J. Neurophysiol.* **52,** 1106–1130.
23. Snowden, R. J., Treue, S. & Andersen, R. A. (1992) *Exp. Brain Res.* **88,** 389–400.
24. Zeki, S. M. (1974) *J. Physiol.* (*London*) **236,** 549–573.
25. Fiorani, M., Jr., Gattass, R., Rosa, M. G. & Sousa, A. P. (1989) *J. Comp. Neurol.* **287,** 98–118.
26. Rosa, M. G. & Elston, G. N. (1998) *J. Comp. Neurol.* **393,** 505–527.
27. Gattass, R., Gross, C. G. & Sandell, J. H. (1981) *J. Comp. Neurol.* **201,** 519–539.
28. Symonds, L. L. & Kaas, J. H. (1978) *J. Comp. Neurol.* **181,** 477–512.
29. Tigges, J., Tigges, M., Anschel, S., Cross, N. A., Letbetter, W. D. & McBride, R. L. (1981) *J. Comp. Neurol.* **202,** 539–560.
30. Weller, R. E., Wall, J. T. & Kaas, J. H. (1984) *J. Comp. Neurol.* **228,** 81–104.
31. Spatz, W. B. (1977) *Exp. Brain Res.* **27,** 559–572.
32. Ungerleider, L. G. & Mishkin, M. (1979) *J. Comp. Neurol.* **188,** 347–366.
33. Huk, A. C., Dougherty, R. F. & Heeger, D. J. (2002) *J. Neurosci.* **22,** 7195–7205.
34. Roy, J. P. & Wurtz, R. H. (1990) *Nature* **348,** 160–162.
35. Roy, J. P., Komatsu, H. & Wurtz, R. H. (1992) *J. Neurosci.* **12,** 2478–2492.
36. Albright, T. D., Desimone, R. & Gross, C. G. (1984) *J. Neurophysiol.* **51,** 16–31.
37. Bonhoeffer, T. & Grinvald, A. (1991) *Nature* **353,** 429–431.
38. Shmuel, A. & Grinvald, A. (1996) *J. Neurosci.* **16,** 6945–6964.
39. Weliky, M., Bosking, W. H. & Fitzpatrick, D. (1996) *Nature* **379,** 725–728.
40. Bonhoeffer, T. & Grinvald A. (1996) in *Brain Mapping: The Methods*, eds. Toga, A. W. & Mazziotta, J. C. (Academic, San Diego), pp. 55–97.